Positron Annihilation in Metallocene Ethylene/1-Hexene Copolymers Related to Their Structure and Mechanical Properties

María L. Cerrada,*,† Ernesto Pérez,† José M. Pereña,† Rosario Benavente,† Marijka Misheva,‡ and Todor Grigorov§

Instituto de Ciencia y Tecnología de Polímeros (CSIC), Juan de la Cierva 3, 28006 Madrid, Spain; Faculty of Physics, Department of General Physics, Sofia University "Kl. Ohridsky", James Bourchier blvd. 5, 1126 Sofia, Bulgaria; and Institute of Nuclear Research and Nuclear Energy, 72 Tzarigradsko Shoosse Blvd, 1784 Sofia, Bulgaria

Received May 4, 2005; Revised Manuscript Received July 19, 2005

ABSTRACT: Positron lifetime measurements are reported for a linear polyethylene and several ethylene−1-hexene copolymers synthesized with metallocene catalysts. The lifetimes, their intensity, the relaxation time, and the relative free volume fraction obtained are correlated with comonomer content, crystallinity, location of β relaxation, and some mechanical parameters, such as elastic modulus and microhardness. A structural discontinuity is found with comonomer molar fraction that evidences the existence of two different regimes: the first one including the homopolymer and copolymers with contents up to around 5−7 mol % and the second regime for higher compositions. Possible reasons for this behavior are discussed. In addition, a linear relationship is found between the location of the β relaxation, which is associated with large-scale cooperative motions in the amorphous environments, and the free volume fraction: the higher the relaxation temperature is, the lower free volume value is obtained.

Introduction

The use of metallocene catalysts has allowed new developments in the field of polyolefins in the past decade. This novel generation of single-site metallocene catalysts leads to copolymers with a homogeneous comonomer distribution along the chain as well as a narrow molecular weight distribution. Moreover, the very high activities of metallocene catalysts allow to incorporate high contents of comonomer in the case of copolymers with different α-olefins, which are difficult to be incorporated with the classical Ziegler−Natta catalysts.

On the other hand, the extraordinary ability of metallocene catalysts to polymerize and copolymerize new monomers enables to synthesize new families of materials that are eliminating the differences between the so-called commodity and engineering polymers and, also, between thermoplastics and elastomers. Consequently, the final physical and mechanical properties of polyethylene and polypropylene might be drastically changed by copolymerization with small amounts of α-olefins. These modifications[1−5] do depend primarily not only on the amount of counits but also on their distribution along the chain and even the nature and length of the side branches arising from the α-olefin.

The measurement of parameters relating to free volume within polymeric systems is an important aspect of their characterization. Free volume can be correlated with such macroscopic properties as diffusion, aging, plasticization, and mechanical properties. Therefore, the behavior of the polyolefin copolymers previously mentioned depend, in a great manner, on the microstructure of the subnanometer local free volume holes: it has to be considered that, for high comonomer contents, an irregular packing and low levels of crystallinity are developed in these materials.[6] Although the concept of free volume in polymers is known for a long time, this topic remains conceptually complex, and a relatively limited amount of experimental data has been reported, mainly those obtained by positron annihilation that is a well-established technique for studying atomic and subnanometer size voids in solids.[7,8]

The basis of the positron annihilation lifetime (PAL) spectroscopy involves the injection of subatomic positrons into the material of interest. A positron of several hundred keV energy from a radioactive source, such as ^{22}Na, becomes thermalized in about 10^{-12} s after entering a solid matter due to ionization and excitation of encountered atoms and molecules. The thermalized positron can (i) annihilate as free particle with one electron within 100−200 ps—as a result, two γ-rays appear; (ii) be trapped at a vacancy-type defect, if latter is neutral or negatively charged; or (iii) form a hydrogen-like bound state (positronium atom, Ps) with an ambient electron. Ps atoms have two different spin states: orthopositronium (o-Ps) and parapositronium (p-Ps) with parallel and antiparallel spins of positron and electron, respectively. The self-annihilation lifetime of p-Ps is 125 ps, while o-Ps lives in a vacuum about 140 ns. In condensed matter, however, the positron from o-Ps may annihilate with one of the opposite-spin surrounding electrons, the so-called pick-off process. In this case, o-Ps lifetime shortens to several nanoseconds. In recent years the positronium atom is widely used to probe atomic-scale free volume holes (pores) in polymers[9] due to the o-Ps property to be localized in empty spaces in condensed matter.

Some previous works have analyzed the effect of the different copolymerization variables in metallocene-catalyzed polyethylene homopolymer and its copolymers with 1-hexene, and their structure has been associated with different properties.[3,10−16] The aim of this new

† Instituto de Ciencia y Tecnología de Polímeros (CSIC).
‡ Sofia University "Kl. Ohridsky".
§ Institute of Nuclear Research and Nuclear Energy.
* Corresponding author: Ph 34-91-5622900, Fax 34-91-5644853, e-mail mlcerrada@ictp.csic.es.

10.1021/ma050938i CCC: $30.25
Published on Web 09/09/2005

Table 1. Characteristics of the Ethylene Copolymers Analyzed: Comonomer Content, Molecular Weight ($M_w \times 10^{-3}$), Melting Temperature (T_m), Crystallinity (f_c^{DSC} and f_c^{WAXD}), Long Spacing (L), Crystal Size (l_c), Density, and Location of β Relaxation (T_β^{DMTA})

samples	1-hexene (mol %)	$M_w \times 10^{-3}$	T_m (°C)	f_c^{DSC}	f_c^{WAXD}	L (nm)	l_c (nm)	density (g/cm^3)	T_β^{DMTA} (°C)
MPE202	0	202	131	0.62	0.68	28.8	19.6	0.949 94	
CEH0.5	0.5	119	126	0.56	0.61	19.7	12.0	0.936 94	−8
CEH1.1	1.1	116	122	0.52	0.55	17.1	9.4	0.933 71	−10
CEH2.0	2.0	113	115	0.42	0.53	14.8	7.8	0.920 64	−15
CEH4.2	4.2	108	100	0.36	0.53	12.8	5.5	0.908 84	−24
CEH8.0	8.0	88	84	0.23	0.33			0.896 22	−45
CEH11.0	11.0	77	67	0.14	0.24	12.7	3.0	0.884 17	−47
CEH14.2	14.2	52	54	0.06	0.09			0.864 83	−53
CEH17.2	17.2		45	0.04	0.08				−55

paper is to study the local free volume holes by positron annihilation methods in a family of ethylene−1-hexene copolymers synthesized with metallocene catalysts. In addition, the size and concentration of these holes have been correlated to some structural and mechanical characteristics in these metallocenic ethylene/1-hexene copolymers. For the first purpose, measurements of positron annihilation lifetime (PAL) have been performed whereas the relationships have been established from measurements of density, X-ray diffraction, differential scanning calorimetry (DSC), dynamic-mechanical thermal analysis (DMTA), uniaxial tensile stress−strain, and microhardness.

Experimental Part

Two sets of ethylene−1-hexene copolymers are analyzed: (a) three metallocenic grades from the pilot plant (CEH0.5, CEH1.1, and CEH2.0) supplied by Repsol YPF and a homopolymer (mPE202) and (b) five other copolymers (CEH4.2, CEH8.0, CEH11.0, CEH14.2, and CEH17.2), synthesized in laboratory using also a metallocene−catalyst system. The copolymerization conditions have been already described elsewhere.[10,11] Table 1 shows the composition in 1-hexene (determined by means of ^{13}C NMR spectroscopy), the molecular weight (by gel permeation chromatography), and other characteristics of the different copolymers.

The films of homopolymer and different copolymers were prepared by compression-molding between hot plates (about 20 °C above the melting temperature) in a Collin press at a pressure of about 2 MPa. The samples were cooled between water plates at the same pressure. The thickness of the molded sheets was around 0.20 mm.

Wide-angle X-ray diffraction (WAXD) patterns were recorded in the reflection mode at room temperature by using a Philips diffractometer with a Geiger counter, connected to a computer. Ni-filtered Cu Kα radiation was used. The diffraction scans were collected over a period of 20 min in the range of 2θ values from 3° to 43°, using a sampling rate of 1 Hz. The goniometer was calibrated with a silicon standard. The samples were also studied by small-angle X-ray scattering (SAXS) employing synchrotron radiation (with $\lambda = 0.150$ nm) in the beamline A2 at HASYLAB (Hamburg, Germany). A SAXS linear position-sensitive detector was used at a distance of 235 cm from the sample and was calibrated with the different orders of the long spacing of rat-tail cornea ($L = 65$ nm). It was found to cover a spacings range from 5 to 55 nm. The crystallite size in the direction normal to the lamellae, l_c, has been estimated from the Lorentz-corrected long spacing, L, and the total crystallinity of the samples by assuming a two-phase model.

The crystalline diffractions and the amorphous component have been separated with a fitting program which allows estimating crystallinity of the samples. The baseline has been just taken as a straight line in the 2θ range from 10° to 30°, and no further correction has been applied. The different diffraction peaks were fitted to Voigt functions. The amorphous peak of the different samples[15] was found to be centered at 2θ between 19.5° and 19.8°.

Table 2. Parameters Obtained from the Mechanical Characterization−Elastic Modulus (E) and Microhardness (MH)−and Positron Annihilation−Intensity Independent of Measurement Path ($I_3(0)$), Pore Volumes (V_p), and Free Volume Fraction (f_V)

samples	1-hexene (mol %)	E (MPa)	MH (MPa)	$I_3(0)$ (%)	V_p (Å^3)	f_V (arb units)
mPE202	0	774	42.5	21.64(48)	134.6	25.4
CEH0.5	0.5	496	34.2	24.00(10)	132.1	30.0
CEH1.1	1.1	364	26.6	25.39(43)	133.3	32.3
CEH2.0	2.0	217	18.2	27.00(25)	137.2	35.3
CEH4.2	4.2	74	6.0	27.50(1.1)	146.4	37.4
CEH8.0	8.0	25	3.5	32.61(9)	156.0	50.9
CEH11.0	11.0	15	1.7	33.93(11)	163.1	54.9
CEH14.2	14.2		1.3	32.78(8)	173.3	56.9
CEH17.2	17.2			33.54(10)	173.4	58.1

Densities, ρ, of the distinct specimens in the solid state were determined at 23 °C in a water−ethanol gradient column which had been calibrated with glass floats.

Thermal properties were determined with a Perkin-Elmer DSC-7 calorimeter connected to a cooling system and calibrated with different standards. The heating rate used was 10 °C/min. For crystallinity determinations, a value of 290 J g^{-1} was taken as the enthalpy of fusion of a perfectly crystalline material.[17]

Dynamic mechanical relaxations were studied with a Polymer Laboratories MK II dynamic mechanical thermal analyzer, working in tensile mode. The storage and loss moduli, E' and E'', respectively, and the loss tangent, tan δ, of each sample were obtained as functions of temperature over the range from −140 to 120 °C at fixed frequencies of 1, 3, 10, and 30 Hz and at a heating rate of 1.5 °C/min.

Stress−strain measurements were performed by using an Instron dynamometer equipped with a load cell and an integrated digital display that provided force determinations. Dumbbell samples with an effective length of 15 mm and a width of 1.9 mm were cut from the compression-molded sheets. These were then subjected to tensile deformation at a constant strain rate of 0.667 min^{-1} and at 23 °C. Elastic modulus, E, was determined from these stress−strain measurements. Because of the inherent uncertainty of data in this type of experiments, at least three specimens of each material have been stretched. The values reported in Table 2 for this mechanical parameter are averages from the different tests.

Microhardness measurements were performed using a Vickers indentor. The microhardness values were calculated from the expression[18]

$$\mathrm{MH} = 2 \sin 68\, P/d^2 \ (\mathrm{MPa}) \qquad (1)$$

where P is the contact load (in N) and d is the length of the diagonal of the indentation surface (in mm). All the measurements were carried out with a load of 0.981 N, and a contact time of 25 s, at room temperature.

Positron Annihilation Lifetime (PAL) Measurements. The positron lifetime measurements were carried out with a standard fast−fast coincidence system. The time resolution function, $G(t)$, is represented as a single Gaussian curve with

full width at half-maximum (fwhm) equal to 0.275 ns. The positron source was ^{22}NaCl between two thin (~7 μm) Kapton foils.

The specimens used for positron annihilation measurements were stacks of thin films, obtained from the compression-molded sheets. All measurements were made in air at room temperature in an air-conditioned laboratory to avoid any electronic drift of the spectrometers used.

The total thickness of the film stacks for some of the materials studied was not sufficient for full absorption of all incident positrons. Because of this, the sample−source−sample sandwich was enclosed between two indium (In) disks. The part of positrons annihilating in the source and in the In disks was taken into account during the spectra processing and was calculated by the program "Layer".[19] The statistics of positrons annihilating only in the samples studied was of the order of 3.5×10^6 counts for each spectrum. At least eight spectra were recorded during 2 days of measurements for each sample.

Each experimental spectrum $N(t)$ is expressed as a convolution of the experimental resolution function $G(t)$ and 3 or 4 negative exponentials $P(t)$ (PATFIT code):

$$N(t) = N_s G(t) P(t);$$

$$P(t) = \sum_1^n \alpha_i \lambda_i \exp(-\lambda_i t) + B \ (i = 3 \text{ or } 4) \quad (2)$$

Here N_s is the total number of annihilation events, λ_i is the annihilation rate, B is the background, and $\alpha_i\lambda_i \equiv I_i$ is the fraction of positrons annihilating with lifetime $\tau_i = 1/\lambda_i$. The sum of relative intensities, I_i, is, of course, equal to 1, $\sum_1^n I_i = 1$.

Lifetime spectra have been also analyzed by the CONTIN-PALS2 program, in which a distribution of annihilation rates is supposed due to heterogeneity of the local environment in which positrons annihilate. In this case the positron lifetime spectrum is expressed by

$$P(t) = \int_0^\infty \lambda \alpha(\lambda) \exp(-\lambda t) d\lambda + B \quad (3)$$

Here $\alpha(\lambda)$ is the annihilation rate probability density function (PDF). To avoid the exact determination of the instrument resolution function, the lifetime spectrum of indium was used as a reference spectrum. Using CONTIN, there is no necessity of making assumptions concerning the number of lifetime components. Moreover, the results from CONTIN can help to choose the proper number of discrete components for PATFIT.

Because of the decrease of the ortho-Ps intensity in the course of measurements, exclusively the last four successive spectra from the whole recorded ones were summed to obtain one spectrum for each sample, with great statistics, analyzed by CONTIN.

Results and Discussion

Characterization of Crystalline and Amorphous Regions. Some features related to crystalline and amorphous fractions of the different specimens (melting temperature, T_m, degree of crystallinity, f_c^{DSC} and f_c^{WAXD}, long spacing, L, crystal size, l_c, and the location of the β relaxation, T_β^{DMTA}) are collected in Table 1, in addition to other molecular parameters previously commented. Determination of crystallinity from WAXD measurements leads, as usual, to f_c^{WAXD} values slightly higher than those from f_c^{DSC}, due to the fact that interfacial content is not contributing to the enthalpy.[20] In addition, it is observed that T_m and f_c decrease with increasing comonomer molar fraction since the lateral butyl branches coming from comonomer cannot be included in the orthorhombic crystalline lattice of polyethylene. Therefore, the presence of comonomer leads to a disruption of the crystallizable units and the formation of smaller and less perfect crystallites (see values of l_c in Table 1).

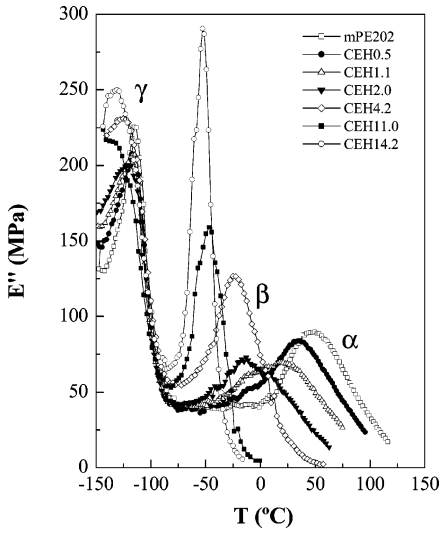

Figure 1. Temperature dependence of the loss modulus (E'') for different specimens under study: mPE202, CEH0.5, CEH1.1, CEH2.0, CEH4.2, CEH11.0, and CEH14.2.

These characteristics associated with the crystalline morphology do deeply affect its counterpart, the amorphous component, in either amount or mobility. The location and intensity of glass transition are commonly good sensors of measuring the effect of crystallites on the mobility of the amorphous regions in semicrystalline polymers. However, if the degree of crystallinity is too high or the glass transition is too close to the melting process in the polymeric system analyzed, the temperature at which its glass transition takes places (T_g) cannot be clearly detected by DSC. In these cases, dynamic mechanical thermal analysis (DMTA) and, more recently, modulated differential scanning calorimetry (MDSC) are useful tools for T_g determination.

Figure 1 shows the relaxation spectra in loss modulus basis at 3 Hz for some of the different specimens. In the samples of lower comonomer content, three different relaxation processes, labeled as γ, β, and α in order of increasing temperatures, are observed. The latest one is associated with vibrational and reorientational motions within the crystallites.[21,22] The temperature location of this relaxation, T_α, has been found in polyethylenes to be very much dependent on the crystal thickness;[23] therefore, T_α is moved to considerably lower temperature, and its intensity is diminished with the increase of comonomer content in ethylene copolymers,[3,23,24] as is clearly seen in Figure 1 for mPE202, CEH0.5, CEH1.1, and CEH2.0, due to the reduction in either crystallinity or crystallite size. For the higher comonomer contents, the α relaxation is not clearly observed due to the progressively decrease in intensity and/or to the merging with the β relaxation.

The assignment of the glass transition in polyethylene to the γ or β relaxations has been a matter of continued intensive study as well as widespread disagreement.[25−30] On one hand, some authors, on the basis of experiments of ^{13}C nuclear magnetic resonance, concluded that the β process could not be identified with the glass transition in either branched or linear polyethylene. On the other hand, the relative lack of sensitivity to morphological factors (presence or absence of crystalline fraction) and the magnitude of the activation parameters

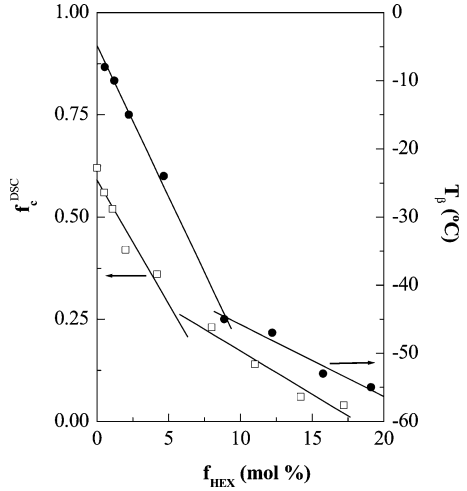

Figure 2. Dependence of DSC crystallinity (left axis) and location of β relaxation (right axis) on comonomer content.

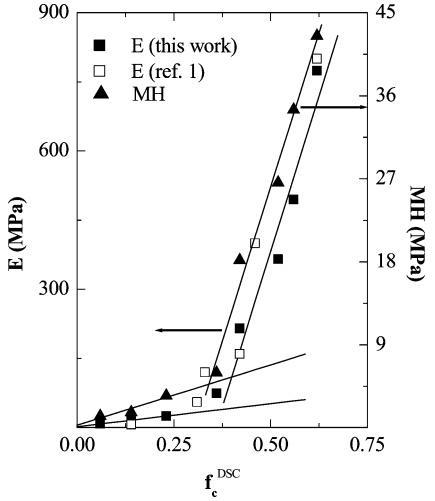

Figure 3. Dependence of elastic modulus (left axis) and microhardness (right axis) on crystallinity. The values of moduli, taken from ref 1, for 1-octene copolymers are also displayed.

have suggested that the γ relaxation has its origin in relatively localized molecular motions.[29] To designate the γ process as the glass transition in linear polyethylene would be justifiable only if one wishes to describe the more prominent amorphous phase relaxation as the glass transition. Molecular dynamics simulations have predicted a volumetric glass transition in amorphous polyethylene associating the β process with the glass transition.[31,32] A T_g of around −50 °C determined by MDSC has been found[33] in an ethylene−1-octene copolymer with a 9.3 mol % 1-octene content and in its composites with glass fiber, and their corresponding β relaxation has been assigned as that associated with cooperative motions.[34] These results are in a perfect agreement with those described for a set of copolymers within a very broad range of compositions.[35]

A clear dependence of the β relaxation on comonomer composition is observed in Figure 1 in the copolymers analyzed. Its location is shifted to lower temperatures, its intensity is considerably raised, and its relaxation time distribution becomes narrower as 1-hexene content is higher in the copolymer. This process has been attributed to a generalized large-scale molecular motion within the amorphous component in these copolymers, similarly to the assumption supposed in the ethylene−1-octene copolymers just mentioned. Therefore, these features are correlated to the increase of overall mobility as crystallinity diminishes and crystallites become less perfect and smaller in size.

Figure 2 represents the influence that comonomer content has, on one hand, on the development of three-dimensional ordered arrangements (f_c^{DSC}) and, on the other hand, on the mobility of the amorphous phase (T_β^{DMTA}). It is clearly observed that the disruption of crystallizable units, already mentioned, leads to the formation of a lesser number of crystallites as comonomer incorporation raises in the copolymer. Obviously, this fact is accompanied by an augment in the amorphous fraction as well as an increase of the mobility of this disordered phase. Consequently, the temperature at which occurs the relaxation associated with the cooperative motions of the amorphous chains is shifted to lower temperatures with the introduction of higher 1-hexene molar compositions. The f_c decrease with composition shows, in principle, a continuous decrease. However, a close approximation displays the existence of two more or less linear behaviors: one for compositions lower than 5 and the other for those equal or higher than 8. This structural discontinuity is again observed in the variation of the mobility within the amorphous domains. (A rather similar trend is observed if f_c^{WAXD} values are taken, considering the analogous decrease of both f_c^{DSC} and f_c^{WAXD}.)

It might be argued that the mentioned discontinuity observed in several magnitudes may be due to the fact that the samples come from two different sources, as explained in the experimental part. However, the CEH4.2 copolymer, corresponding to the "second" group of samples, actually falls in the "first" group behavior.

The physical and mechanical properties of polymeric materials depend on the degree of crystallinity as well as on the crystalline structure and morphology. Therefore, a change in the mechanical parameters is expected for the different copolymers due to the variations within the crystalline and amorphous regions by the insertion of distinct compositions in 1-hexene. The effect of these structural modifications is observed in Figure 3 where the dependence of elastic modulus and microhardness on crystallinity is plotted. A discontinuity in both mechanical parameters is again observed. The copolymers with 1-hexene contents lower than around 5% (crystallinities higher than around 30%) are relatively much more rigid than the other copolymers: it seems that the crystals in the copolymers with higher comonomer contents contribute very little to the mechanical properties.

A division of ethylene−1-octene copolymers as a function of density has been suggested.[1] Such a classification scheme shows a broad range of solid-state structures. Copolymers with densities higher than 0.93 g/cm^3 exhibit a lamellar morphology with well-developed spherulitic superstructure. If density values are in the 0.93−0.91 g/cm^3 range, the copolymers have thinner lamellae and smaller spherulites. Materials with densities between 0.91 and 0.89 g/cm^3 have a mixed morphology of small lamellae and bundled crystals. These materials can form small spherulites. And finally, copolymers with densities less than 0.89 g/cm^3 have no lamellae or spherulites: fringed micellar or bundled crystals are inferred from the low degree of crystallinity and the granular, nonlamellar morphology. Supplementary work on very low density copolymers has shown

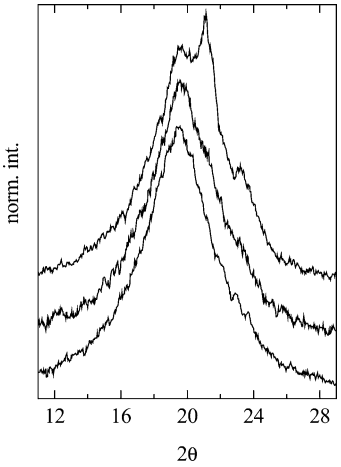

Figure 4. X-ray diffraction patterns at room temperature of CEH11.0, CEH14.2, and CEH17.2 (from top to bottom) shifted vertically for clarity.

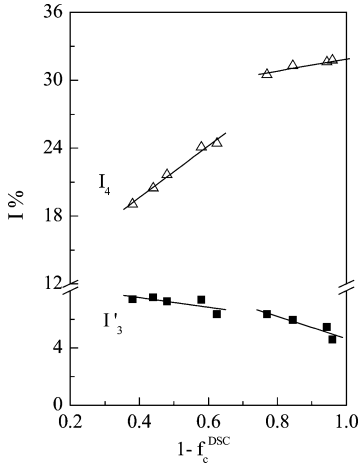

Figure 5. Variation of I_3' and I_4 with amorphous content.

that even copolymers with densities in the range 0.88−0.89 present two crystal populations, attributed to a mixture of lamellar and bundled crystal.[36]

Moreover, a careful analysis of the diffraction profiles corresponding to specimens with high comonomer content indicates that, besides the (110) and (200) reflections typical of the orthorhombic modification of polyethylene, a third crystalline reflection, centered at 0.453 nm, is obtained. This reflection has been attributed to a hexagonal phase more disordered than the orthorhombic one.[4,37] For instance, the analysis in a copolymer with a 9.3 mol % 1-octene shows a total X-ray crystallinity of 22%, which is divided, approximately, in a 9% of disordered hexagonal form and 13% of orthorhombic one.

Similar features seem to be valid for the present ethylene−1-hexene copolymers. In fact, Figure 4 shows the X-ray diffractograms corresponding to the three copolymers with higher comonomer contents (the diffractograms for the other samples have been previously reported[15]). It can be observed that the diagram for sample CEH11.0 exhibits the (110) and (200) reflections of orthorhombic polyethylene crystals, and a peak centered at 19.5° is also observed. On the contrary, the diffractograms for the other two copolymers with higher comonomer content do not exhibit the (110) and (200) reflections, and only the peak centered at 19.5° is observed. This peak is significantly narrower than the one corresponding to a molten sample,[38] so that our interpretation is that they are composed of an amorphous very wide component and a single diffraction (of intermediate width) at the top, assigned to disordered hexagonal crystals. These disordered crystals may be the major constituent of the bundlelike crystals exhibited by these copolymers of very low crystallinity (but yet detectable by DSC). The total crystallinity values deduced from WAXD, as mentioned in the experimental part and commented above, are presented in Table 1.

The contribution of these very imperfect crystals to the total rigidity of the sample seems to be considerably smaller than the one from the "regular" lamellar crystals, judging from the clear break observed in Figure 3 for both the elastic modulus and microhardness. This break occurs when the DSC crystallinity is around 30−35% (a density around 0.90 g/cm^3), which corresponds to the value, as commented above, where a mixed morphology of small lamellae and bundled crystals is obtained. This change in morphology is also accompanied by a different mechanical behavior: the samples with higher comonomer content display deep elastomeric characteristics, and therefore, they are much more ductile and softer.

The parallelism between the present ethylene−1-hexene copolymers and those with 1-octene[1] can be observed in Figure 3: the elastic moduli of the two series of copolymers behave in a very similar manner.

PAL Spectroscopy. Three components appear in the lifetime spectrum of an amorphous polymer. The first one ($\tau_1 \approx 150$ ps) comes from p-Ps self-annihilation. The second term ($\tau_2 \approx 0.4$ ns) is due to annihilation of free (not bound in Ps atom) positrons. These two short-lived components are insensitive to the polymer structure changes.[39,40] The third lifetime constituent (t_3 is of the order of several nanoseconds) is ascribed to o-Ps pick-off annihilation, and it depends on polymer structure.

However, a four-term decomposition of lifetime spectra is often used in semicrystalline polymers. In this case, components appearing at the longest lifetime vary with structural details of the polymeric systems. The third one ($\tau_3' \approx 1$ ns) refers to o-Ps pick-off annihilation at defects localized in crystalline parts of the samples while the longest-lived component (τ_4 of the order of several nanoseconds) is due to pick-off annihilation of o-Ps, localized at free volume holes in amorphous parts. Free volume holes are due to static ($T_{\text{measurement}} < T_g$) or dynamic ($T_{\text{measurement}} > T_g$) structural disorder in the amorphous phase of a polymer. The T_g values of CEH copolymers are within the interval from −8 to −55 °C, so at room temperature, i.e., at the temperature of measurement, $T_{\text{measurement}}$, the free volume holes are related to dynamic disorders.

In the present case, the variances, χ^2, of the fit for a three-term decomposition of the spectra are in the range 1.0−1.8. A better agreement ($\chi^2 \approx 0.95-1.2$) is obtained using an unconstrained four-term decomposition for the fit, although the scatter in lifetimes and their relative intensities were larger to some extent.

The above interpretation of lifetimes τ_3' and τ_4 is consistent with the dependences of their relative intensities I_3' and I_4 on the amorphous fraction $(1 - f_c^{\text{DSC}})$ in the polymers studied, as depicted in Figure 5 (f_c is the DSC degree of crystallinity). As can be seen, I_3' decreases and I_4 increases when the amount of amorphous part in the polymer studied increases. Two different linear regions are again observed, related with the comonomer content. Figure 5 also shows a higher

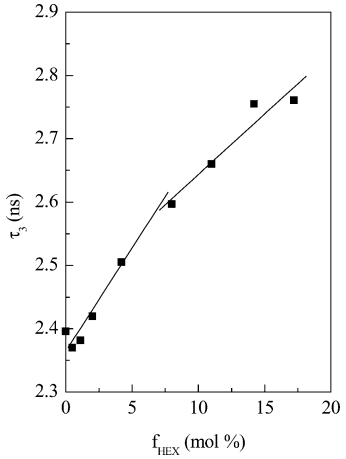

Figure 6. Dependence of lifetime τ_3 on comonomer composition.

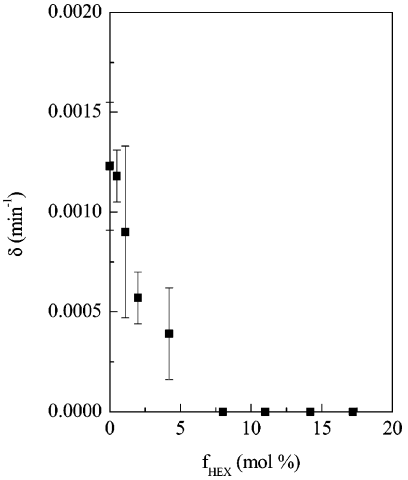

Figure 7. Variation of the relaxation rate with 1-hexene content.

sensitivity of I_4 compared with intensity of the component associated with annihilation at crystalline defects, I_3'.

The mean lifetimes, τ_m, calculated by

$$\tau_m = \sum_1^N \tau_i I_i \quad (N = 3 \text{ and } 4) \tag{4}$$

are the same in the error limits for the two different spectra processing, implying that three- and four-term decompositions are not contradicted. The largest component τ_4 is only 3−6% greater than t_3 obtained from a three-term decomposition of the lifetime spectra, and both τ_3 and τ_4 vary in the same way with comonomer content. Mainly, the results from three-term analysis of the lifetime spectra will be presented and discussed further.

The o-Ps lifetime τ_3 as a function of comonomer content, f_{HEX}, is depicted in Figure 6. It is found to vary linearly with 1-hexene content, but two different regimes can be observed. The τ_3 value of mPE202 homopolymer is in some extent larger than expected from the linear dependence of the copolymers with low 1-hexene content.

As mentioned above, in some of the polymers studied here a decrease of the o-Ps relative intensity I_3 during the period of measurements has been observed, similar to that reported elsewhere.[41,42]

To obtain for each specimen a value of I_3 independent of the particular way of positron lifetime measurement, namely number of repetitions and duration of each measurement, $I_3(t)$ has been fitted to an exponential

$$I_3(t) = I_3(\infty) + [I_3(0) - I_3(\infty)] \exp(-\delta t) \tag{5}$$

where δ is the relaxation rate of $I_3(t)$.

Moreover, two different samples in two independent measurements of the homopolymer mPE202 have been performed under two different protocols to check the influence of the number and way of lifetime measurements on the fitted values from eq 5. The approximation of I_3 with eq 5 gave $I_3(0) = 21.67(48)\%$, $\delta = 0.00123(36)$ min^{-1} and $I_3(0) = 21.67(48)\%$, $\delta = 0.00123(32)$ min^{-1} for the first and second series, respectively. So, although the number and route of measurements are different, the values of $I_3(0)$ and δ obtained are the same. This implies that the attained $I_3(0)$ values may be used to characterize the properties of the polymers studied regardless of the way of positron lifetime measurement.

The relative intensity I_3 of o-Ps pick-off annihilation ceased to depend exponentially on time elapsed from the first contact of positron source and studied samples, i.e. during the period of measurement for CEH copolymers with concentration in 1-hexene equal to or higher than 8 mol %. For these copolymers, $I_3(0)$ was obtained by linear approximation of $I_3(t)$, and δ is considered equal to zero. The $I_3(0)$ values are listed in Table 2, and the relaxation rate, δ, as a function of f_{HEX} concentration is presented in Figure 7.

The commonly accepted explanation of the o-Ps intensity−time dependence is that it is a result of positive charge ceaselessly accumulated in the polymer during PAL measurement and/or competition between formation and disappearance of species, as free radicals and ionized molecules, produced by positrons themselves, which inhibit Ps formation (see ref 9 and references therein). The lifetimes of the mentioned species depend on their mobility. The latter is determined by the temperature, availability of free volume, and is higher as the difference $\Delta T = |T_{measurement} - T_g|$ is larger. In the present case the values of ΔT and pore volumes V_P increase as 1-hexene molar fraction does. This is in our opinion the reason for δ decrease. Similar change of I_3 rate decrease with elapsed time is observed by Dlubek et al. in poly(α-olefin)s.[43]

The values of o-Ps lifetimes are nearly independent of time of measurement.

The ortho-Ps pick-off lifetime t_3 (or τ_3' and τ_4) depends on size of the free volume hole at which the Ps atom is localized before annihilation. The so-called Tao−Eldrup model,[44,45] in which a spherical-shaped pore of radius R has been assumed, gives the following dependence between R and τ_3

$$\tau_3 = \{\lambda_B[1 - (R/R_0) + (1/2\pi)\sin(2\pi R/R_0)]\}^{-1} \tag{6}$$

In this equation, $\lambda_B = 2$ ns^{-1} is the spin average Ps annihilation rate and $R_0 = R + \Delta R$. The thickness, ΔR, of the electron layer on the pore walls, $\Delta R = 0.1656$ nm, was empirically determined in ref 46. Therefore, the volume V_p^s of isolated pores can be determined via $V_p^s = (4/3)\pi R^3$ from the corresponding average pore radii, calculated by eq 6 from the o-Ps lifetimes.

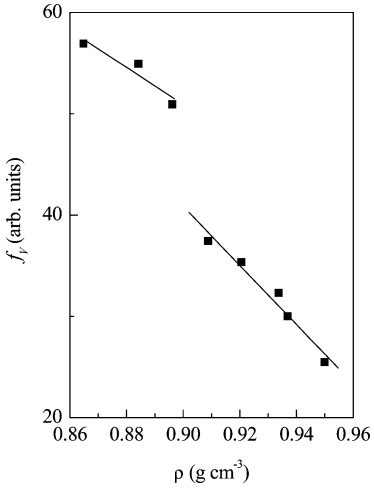

Figure 8. Relationship between free volume fraction and density.

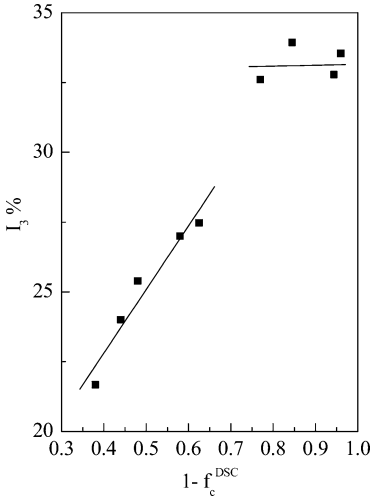

Figure 9. Dependence of I_3 on amorphous content.

The o-Ps intensity is often considered as an estimation of the free volume pore concentration,[9,47] and the relative free-volume fraction F_V is expressed by

$$F_V = CI_3V_p^s \tag{7}$$

where C is a parameter, extracted usually from pressure−volume−temperature (PVT) measurements. If the value of C can be considered identical for all polymers here studied, the parameter $f_V = I_3V_p^s$ can be used as a quantity proportional to the fractional free volume. The latter is defined by $F_V = V_p/(V_p + V_m)$, where V_p and V_m are the volumes of the all pores and solid phase holding in a given volume $V = V_p + V_m$ of the material studied. The specific pore volume V_S^{pore} (cm^3/g) $= V_p/V_m\rho_m$ according to Brinker et al.[48] can be depicted by $V_S^{pore} = 1/\rho - 1/\rho_m$, where ρ and ρ_m are the bulk and solid phase densities, respectively, supposing that all of the free volume is spatially together in the latest density. The fractional free volume F_V can be expressed by V_S^{pore}: $F_V = V_p/V = \rho V_S^{pore}$, and $F_V \approx 1 - \rho/\rho_m$. If ρ_m is considered as equal and constant for all samples studied, then f_V will be a linear function of ρ.

The values of f_V vs density are depicted in Figure 8. Two different linear intervals are again observed: the specimens with densities higher than about 0.90 g cm^{-3} follow a well different straight line than those of lower densities.

In connection with eq 7 some additional remarks are needed. First of all, this equation may be applied only for polymers that do not contain groups, which are scavengers of electron or/and positrons. On the other side, the o-Ps intensity decreases with time elapsed from the beginning of PAL measurements of each studied sample. As discussed above, this is explained by accumulation of species, which inhibit Ps formation. To overcome this difficulty, the $I_3(0)$ values obtained by eq 5 were used in eq 7, since at the very beginning of a sample measurement there is no inhibition.[49]

The scaling constant C in eq 7 expresses the probability of o-Ps formation that does not depend on free volume. As the macromolecules of the studied copolymers contain the same repeating units, there is no reason to consider that C will have a variety of values for different copolymers.

Using o-Ps as a probe of free volume studies of polymers, the free volume could be either observed (V_o) or unobserved (V_{uo}) with o-Ps, depending on their size: if they are macroscopic defects, larger than the angstrom scale, they cannot be observed by o-Ps atoms. The polymer density is determined from both free volumes, while the parameter f_V should depend only on V_o. In other words, if f_V linearly decreases with density increase, this means that I_3 is a measure of pore concentration and, additionally, that there are not macroscopic defects in the samples studied. The opposite statement is also valid; i.e., if I_3 is not a measure of pore concentration and/or if macroscopic defects larger than angstrom scale exist in the samples, then f_V and ρ are not linearly dependent. From the linear behavior observed in Figure 8, it follows that in the present case I_3 could be considered as a measure of the concentration of pores.

The o-Ps intensity I_3 varies linearly with the amount of amorphous phase in the copolymers studied, as seen in Figure 9. As well, two linear regimes with composition and, therefore, with amorphous fraction are observed. The extrapolation of linear dependence from samples with low comonomer content to a fully crystalline specimen leads to an I_3 value of 12.8%. As discussed above, this can be explained[40,50] considering that Ps atoms may be formed not only in amorphous but also in crystalline parts of semicrystalline polymers. The value obtained for I_3 is somewhat larger than the one of I_3' obtained by unconstrained four-component fit of the lifetime spectra.

In fact, as discussed by Dlubek et al.,[51] the conception of only two phases, crystalline and amorphous, in semicrystalline polymers is a too simplified one. At least a three-phase model, which includes the crystal/amorphous interface, should be regarded as more corresponding to the reality. The free volume holes at which o-Ps atoms annihilate are localized both in amorphous regions and in the crystal/amorphous interface. Obviously, it could not be expected that the crystal fold surface in the present case of CEH copolymers is an ordered one, since the butyl branches are excluded from the crystallites. The rejected counits aggregate, resulting in a "switchboard" appearance of the lamella fold surface. It is reasonable to suppose that the disorder of the interface grows up with increasing comonomer content. Accordingly, the relative part of o-Ps atoms that annihilate at free volume holes localized in the crystal/amorphous interface also increases. In our opinion this is the reason for different slopes of I_3 (and I_4 from Figure

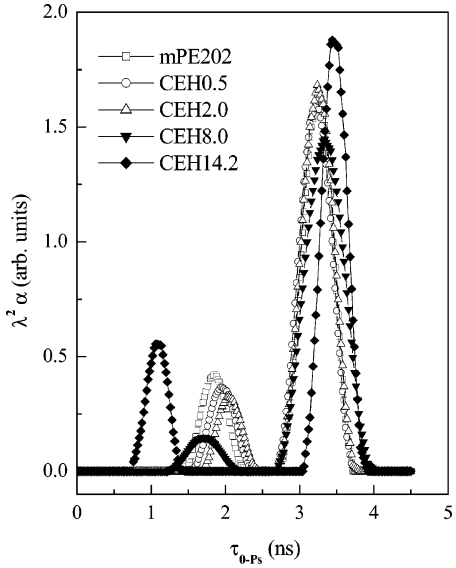

Figure 10. Positron lifetime distributions from the lifetime spectra of different copolymers analyzed.

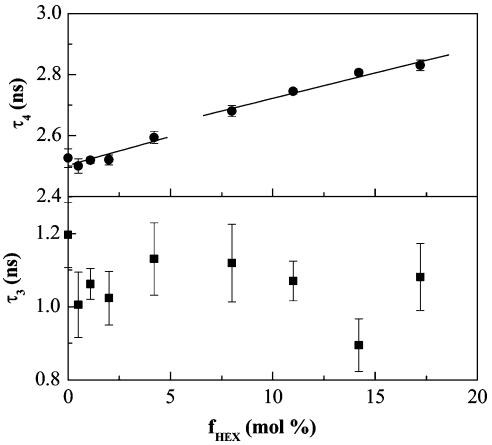

Figure 11. Dependences of lifetimes τ_3 and τ_4 on comonomer content.

5) for samples with different comonomer content. The discontinuity of I_3 (I_4) = $f(1 - f_c^{DSC})$ occurs at the same 1-hexene molar composition as for the other copolymer characteristics.

As mentioned above, the lifetime spectra have been also processed by the CONTIN program. Two o-Ps lifetime distributions have been observed for all of the specimens studied, as depicted in Figure 10 for some of the CEH copolymers. This observation urged us to probe the unconstrained four-term decomposition of the lifetime spectra (see above). As already mentioned, this procedure drives to χ^2 reduction, but also to a considerable scatter in the I_3', τ_3', I_4, and τ_4 values. Nevertheless, it is interesting to follow the trends of o-Ps intensities as functions of amorphous phase content $(1 - f_c^{DSC})$ of polymers studied (Figure 5). As can be seen, I_3' values decrease, while I_4 values increase with $(1 - f_c^{DSC})$ increasing. Such trend could be expected if the latter intensity is connected with amorphous and the former one with the crystalline regions of polymers.

The τ_3' values are in the range 1−1.5 ns, while τ_4 is in the range 2.5−2.8 ns. Ortho-Ps lifetimes as functions of comonomer concentration are presented in Figure 11. The τ_4 lifetimes increase with comonomer content, and two linear behaviors are shown. However, there is not a clear dependence for τ_3' in these CEH copolymers.

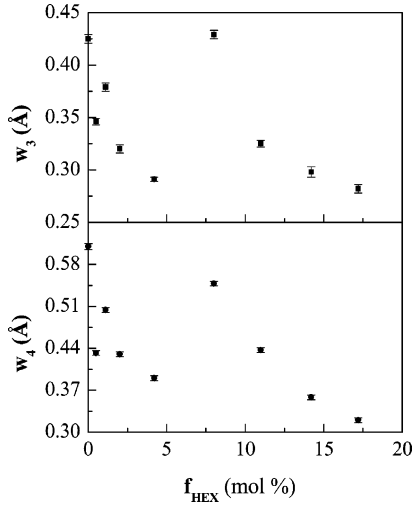

Figure 12. Variation of the widths w_3 and w_4, with the comonomer content.

These features might be interpreted as an indication that the interaction between macromolecules in amorphous parts of the polymers studied decreases with adding of comonomer, while in the crystalline phase of CEH there is no indication of such change.

Pore radius distributions (Figure 10) point out the heterogeneity of the local environment of the annihilating o-Ps atom. The distribution have been approximated by Gaussians

$$f(R) = \text{const} + \frac{A}{w\sqrt{\pi/2}} \exp\left(\frac{-2(R - R_C)^2}{w^2}\right) \qquad (8)$$

using the program package ORIGIN 4.1. The obtained values for widths w_3 and w_4 of radii R_3' and R_4, respectively, are presented in Figure 12. As can be seen, the samples studied could be classified into two groups depending upon composition, as we have already discussed for another structural and mechanical parameters: those for lower contents of comonomers and, therefore, high values of crystallinity and those with 1-hexene compositions equal to or higher than 8%. In each group, w_3 and w_4 decrease as comonomer increases. This feature implies that the sizes of pores, related to those existing within the crystalline (w_3) and amorphous (w_4) parts, become more uniform, and therefore, the distribution width is reduced. In addition, as expected, the pore radius distributions in crystalline phase (w_3) of a particular material are always narrower than those in the amorphous phase (w_4).

Finally, Figure 13 shows the relationship between the free volume fraction and the location of the relaxation related to cooperative motions within the amorphous regions. A significant increase of free volume amount is observed when the amorphous content increases, as also reported in Table 2. It seems that now a single straight line is obtained, meaning that a direct relationship exists between these two variables. It is noticeable, however, the wide gap observed between the two kinds of samples: those of low comonomer content (with a lamellar spherulitic morphology) and the ones with high comonomer content (exhibiting bundlelike crystals and a majority of disordered hexagonal crystals). The change in morphology seems to be responsible, therefore, for a very high increase of the free volume fraction, and as a direct result, the β relaxation appears at considerably

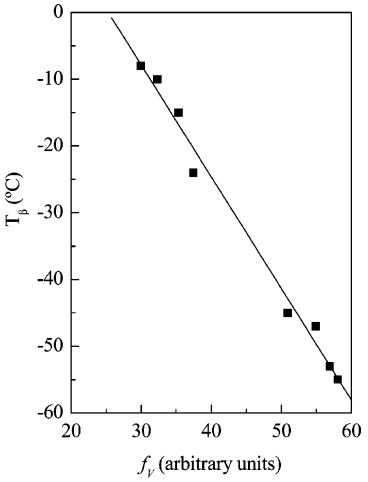

Figure 13. Relationship between maximum temperature of β relaxation and parameter f_V, proportional to free volume fraction.

lower temperatures for the group of copolymers with high comonomer contents.

A final aspect from Figure 13 is that, assuming the depicted linear relationship, a extrapolated value of around 0 °C would be obtained for the β relaxation of the studied polyethylene homopolymer sample, from the known value of 25.4 for its free volume fraction (see Table 2).

Conclusions

A structural discontinuity is observed within the set of ethylene−1-hexene copolymers analyzed. Thus, the variation of crystallinity and the mobility of the amorphous regions with the comonomer composition show two different linear dependences: one up to 1-hexene contents of around 5−7 mol % and another for higher molar fractions. This feature is probably associated with changes in morphological aspects within the copolymers. Those included in the former regime present a lamellar morphology with well-developed spherulitic superstructure, though the lamellae become thinner and spherulites smaller as 1-hexene content increases. However, a mixed morphology of small lamellae and bundled crystals is developed in copolymers with comonomer contents equal to or higher than 8 mol %, similarly to that found in ethylene−1-octene copolymers. Moreover, a careful analysis of the diffraction profiles corresponding to specimens with high comonomer content indicates that, besides the (110) and (200) reflections typical of the orthorhombic modification of polyethylene, a third crystalline reflection, centered at 0.453 nm, is obtained that is attributed to a hexagonal phase more disordered than the orthorhombic one. All these structural characteristics do deeply affect the mechanical response and the parameters estimated by positron annihilation. Therefore, these two linear behaviors with composition or related magnitudes are observed in the variation of elastic modulus, microhardness, o-Ps lifetimes and their intensities, relaxation rates, and free volume fractions.

Acknowledgment. The authors are grateful for the financial support of Comunidad Autónoma de Madrid, Ministerio de Educación y Ciencia, and the Exchange Collaboration Program Bulgarian Academy of Sciences and the Spanish Council for Scientific Research (projects 07/0093/2002 and GR/MAT/0728/2004, MAT2004-01547, and 2004BG0009, respectively). The support from the European Commission (COST Action D17, WG D17/0004/00) is also acknowledged. The synchrotron work (in the A2 polymer line of Hasylab at DESY, Hamburg) was supported by the European Community−Research Infrastructure Action under the FP6 "Structuring the European Research Area" Programme (through the Integrated Infrastructure Initiative "Integrating Activity on Synchrotron and Free Electron Laser Science") (Contract RII3-CT-2004-506008). We thank the collaboration of the Hasylab personnel, especially Dr. S. Funari. Finally, we acknowledge the support from International Atomic Energy Agency (Research Agreement 12705/RO).

References and Notes

(1) Bensason, S.; Minick, J.; Moet, A.; Chum, S.; Hiltner, A.; Baer, E. *J. Polym. Sci., Polym. Phys. Ed.* **1996**, *34*, 1301.
(2) Mathot, V. B. F.; Scherrenberg, R. L.; Pijpers, T. F. J. *Polymer* **1998**, *39*, 4541.
(3) Cerrada, M. L.; Benavente, R.; Peña, B.; Pérez, E. *Polymer* **2000**, *41*, 5957.
(4) Cerrada, M. L.; Benavente, R.; Pérez, E. *J. Mater. Res.* **2001**, *16*, 1103.
(5) Palza, H.; López-Majada, J. M.; Quijada, R.; Benavente, R.; Pérez, E.; Cerrada, M. L. *Macromol. Chem. Phys.*, in press.
(6) Dlubek, G.; Bamford, D.; Henschke, O.; Knorr, J.; Alam, M. A.; Arnold, M.; Lüpke, T. *Polymer* **2001**, *42*, 5381.
(7) Pethrick, R. A. *Prog. Polym. Sci.*. **1997**, *22*, 1.
(8) Dlubek, G.; Kilburn, D.; Bondarenko, V.; Pionteck, J.; Krause-Rehberg, R.; Alam, M. A. *Macromol. Symp.* **2004**, *210*, 11.
(9) Mallon, P. E. In *Principals and Application of Positron and Positronium Chemistry*; Jean, Y. C., Mallon, P. E., Schrader, D. M., Eds.; World Scientific Press: Singapore, 2003; p 253.
(10) Quijada, R.; Dupont, J.; Miranda, M. S. L.; Scipioni, R. B.; Galland, G. B. *Macromol. Chem. Phys.* **1995**, *196*, 3991.
(11) Quijada, R.; Galland, G. B.; Mauler, R. S. *Macromol. Chem. Phys.* **1996**, *197*, 3091.
(12) Simanke, A. G.; Galland, G. B.; Neto, R. B.; Quijada, R.; Mauler, R. S. *J. Appl. Polym. Sci.* **1999**, *74*, 1194.
(13) Simanke, A. G.; Galland, G. B.; Freitas, L. L.; da Jornada, J. A. H.; Quijada, R.; Mauler, R. S. *Macromol. Chem. Phys.* **2001**, *202*, 172.
(14) Villar, M. A.; Failla, M. D.; Quijada, R.; Mauler, R. S.; Valles, E. M.; Galland, G. B.; Quinzani, L. M. *Polymer* **2001**, *42*, 9269.
(15) Laguna, M. F.; Cerrada, M. L.; Benavente, R.; Pérez, E. *J. Membr. Sci.* **2003**, *212*, 167.
(16) Laguna, M. F.; Cerrada, M. L.; Benavente, R.; Pérez, E. *J. Polym. Sci., Polym. Phys. Ed.* **2003**, *41*, 2174.
(17) Flory, P. J.; Vrij, A. *J. Am. Chem. Soc.* **1961**, *85*, 3548.
(18) Baltá-Calleja, F. J. *Adv. Polym. Sci.* **1985**, *66*, 117.
(19) Djourelov, N.; Misheva, M. *J. Phys.: Condens. Matter* **1996**, *8*, 2081.
(20) Alamo, R.; Domszy, R.; Mandelkern, L. *J. Chem. Phys.* **1984**, *88*, 6587.
(21) McCrum, N. G.; Read, B. E.; Williams, G. *Anelastic and Dielectric Effects in Polymeric Solids*; Dover Publication: New York, 1991; Chapter 10, p 353.
(22) Ward, I. M. *Mechanical Properties of Solids Polymers*, 2nd ed.; John Wiley and Sons: Chichester, 1985; Chapter 8, p 166.
(23) Popli, R.; Glotin, M.; Mandelkern, L.; Benson, R. S. *J. Polym. Sci., Polym. Phys. Ed.* **1984**, *22*, 407.
(24) Martínez-Burgos, J. M.; Benavente, R.; Pérez, E.; Cerrada, M. L. *J. Polym. Sci., Polym. Phys. Ed.* **2003**, *41*, 1244.
(25) Stehling, F. C.; Mandelkern, L. *Macromolecules* **1970**, *3*, 342.
(26) Boyer, R. F. *Macromolecules* **1973**, *6*, 228.
(27) Davis, G. T.; Eby, R. K. *J. Appl. Phys.* **1973**, *44*, 4274.
(28) Dechter, J. J.; Axelson, D. E.; Dekmezian, A.; Glotin, M.; Mandelkern, L. *J. Polym. Sci., Polym. Phys. Ed.* **1982**, *20*, 641.
(29) Boyd, R. H. *Macromolecules* **1984**, *17*, 903.
(30) Han, J.; Gee, R. H.; Boyd, R. H. *Macromolecules* **1994**, *27*, 7781.
(31) Boyd, R. H.; Gee, R. H.; Han, J.; Jin, Y. *J. Chem. Phys.* **1994**, *101*, 788.
(32) Jin, Y.; Boyd, R. H. *J. Chem. Phys.* **1998**, *108*, 9912.

(33) Cerrada, M. L.; Benavente, R.; Pérez, E.; Moniz-Santos, J.; Ribeiro, M. R. *Polymer* **2001**, *42*, 7197.
(34) Cerrada, M. L.; Benavente, R.; Pérez, E. *Macromol. Chem. Phys.* **2002**, *203*, 718.
(35) Vanden Eynde, S.; Mathot, V. B. F.; Koch, M. H. J.; Reynaers, H. *Polymer* **2000**, *41*, 4889.
(36) Minick, J.; Moet, A.; Hiltner, A.; Baer, E.; Chum, S. P. *J. Appl. Polym. Sci.* **1995**, *58*, 1371.
(37) Androsch, R.; Blackwell, J.; Chvalun, S. N.; Wunderlich, B. *Macromolecules* **1999**, *32*, 3735.
(38) Pérez, E.; Benavente, R.; Quijada, R.; Narvaez, A.; Galland, G. B. *J. Polym. Sci., Polym. Phys. Ed.* **2000**, *38*, 1440.
(39) Hristov, H. A.; Bolan, B.; Yee, A. F.; Xie, L.; Gidley, D. W. *Macromolecules* **1996**, *29*, 8507.
(40) Dlubek, G.; Bamford, D.; Rodríguez-González, A.; Bornemann, S.; Stejny, J.; Schade, B.; Alam, M. A.; Arnold, M. *J. Polym. Sci., Polym. Phys. Ed.* **2002**, *40*, 434.
(41) Suzuki, T.; He, C.; Kondo, K.; Shantarovich, V.; Ito, Y. *Radiat. Phys. Chem.* **2003**, *68*, 489.
(42) Maurer, F. H. J.; Schmidt, M. *Radiat. Phys. Chem.* **2000**, *58*, 509.
(43) Dlubek, G.; Bamford, D.; Henschke, O.; Knorr, J.; Alam, M. A.; Arnold, M.; Lupke, T. *Polymer* **2001**, *42*, 5381.
(44) Eldrup, M.; Lightbody, D.; Sherwood, J. N. C*hem. Phys.* **1981**, *63*, 51.
(45) Tao, S. J. *J. Chem. Phys.* **1972**, *56*, 5499.
(46) Nakanishi, H.; Wang, S. J.; Jean, Y. C. *Positron Annihilation Studies of Fluids*; Sharma, S. C., Ed.; World Scientific: Singapore 1988; p 292.
(47) Kobayashi, Y.; Zheng, W.; Meyer, E. F.; McGervey, J.; Jamieson, A. *Macromolecules* **1989**, *22*, 2302.
(48) Brinker, C. J.; Scherer, G. W.; Roth, E. P. *J. Non-Cryst. Solids* **1985**, *72*, 345.
(49) Djourelov, N.; He, C.; Suzuki, T.; Shantarovich, V. P.; Ito, Y.; Kondo, K.; Ito, Y. *Radiat. Phys. Chem.* **2003**, *68*, 689.
(50) Nakanishi, H.; Jean, Y. C.; Smith, E. G.; Sandreczki, T. C. *J. Polym. Sci., Polym. Phys. Ed.* **1989**, *27*, 1419.
(51) Dlubek, G.; Stejny, J.; Lupke, T.; Bamford, D.; Petters, K.; Hubner, C.; Alam, M. A.; Hill, M. J. *J. Polym. Sci., Polym. Phys. Ed.* **2002**, *40*, 65.

MA050938I